



ELSEVIER

Polymer 44 (2003) 857–866

polymerwww.elsevier.com/locate/polymer

New polylactide-layered silicate nanocomposites. 2. Concurrent improvements of material properties, biodegradability and melt rheology

Suprakas Sinha Ray^a, Kazunobu Yamada^b, Masami Okamoto^{a,*}, Kazue Ueda^b^a*Advanced Polymeric Materials Engineering, Graduate School of Engineering, Toyota Technological Institute, Hisakata 2-12-1, Tempaku, Nagoya 468 8511, Japan*^b*Unitika Ltd, Kozakura 23, Uji, Kyoto 611-0021, Japan*

Received 15 July 2002; received in revised form 4 September 2002; accepted 15 October 2002

Abstract

Our continuing research on the preparation, characterization, materials properties, and biodegradability of polylactide (PLA)-layered silicate nanocomposites has yielded results for PLA–montmorillonite nanocomposites. Montmorillonite modified with trimethyl octadecylammonium cation was used as an organically modified layered silicate for the nanocomposites preparation. The internal structure of the nanocomposites in the nanometer range has been established by using wide-angle X-ray diffraction and transmission electron microscope analyses. All the nanocomposites exhibited superior improvement of practical materials properties such as storage modulus, flexural modulus, flexural strength, heat distortion temperature, and gas barrier property as compared to that of neat PLA. The biodegradability of neat PLA and a representative nanocomposite was also studied under compost, and the rate of biodegradation of neat PLA significantly increased after nanocomposites preparation. The melt rheology of neat PLA and various PLACNs was also studied.

© 2002 Elsevier Science Ltd. All rights reserved.

Keywords: Polylactide-layered silicate nanocomposites; Materials properties; Biodegradability

1. Introduction

Now a days tremendous amounts and varieties of plastics, notably polyolefins, polystyrene and poly(vinyl chloride), are produced mostly from fossil fuels, consumed and discarded into the environment, ending up as spontaneously *undegradable* wastes. Their disposal by incineration some time produces toxic gases and contributes to global pollution, and satisfactory landfill sites are also limited. For these reasons, there is an urgent need for the development of ‘green polymeric materials’ that would not involve the use of toxic or noxious components in their manufacture, and could allow to composting to naturally occurring degradation products. Accordingly PLA is of increasing interest because it is made from renewable sources and its properties are benign to the environment [1–5].

PLA is a linear aliphatic thermoplastic polyester, produced by the ring-opening polymerization of lactides

and the lactic acid monomers, which are obtained from the fermentation of sugar feed stocks, corn, etc. [6]. PLA has high mechanical, thermal plasticity, fabric-ability, and biocompatibility. So PLA is a promising polymer for various end-use applications [7]. However, some of the other properties such as melt viscosity, impact factor, heat distortion temperature (HDT), gas barrier properties, etc. are frequently not enough for various end-use applications [8].

In recent time, the intercalation of polymers from either solution or the melt in the silicate galleries of clay is the best technique to prepare nanocomposites material which often exhibit remarkable improvement of mechanical, thermal, optical and physicochemical properties [9–16] when compared with the pure polymer or conventional composites (micro- and macro-composites). Additionally, these nanocomposites have been proposed as model systems to examine polymer structure and dynamics in confined environments [17,18]. On the other hand, layered silicate is naturally abundant, economic, and more importantly benign to the environment.

In our recent paper [19], we have reported the successful preparation of PLA-organically modified layered silicate

* Corresponding author. Tel.: +81-52-809-1861; fax: +81-52-809-1864.
E-mail address: okamoto@toyota-ti.ac.jp (M. Okamoto).

(OMLS) nanocomposites by melt extrusion of PLA and montmorillonite (mmt) modified with octadecylammonium cation (C_{18} -mmt). Wide-angle X-ray diffraction (WAXD) analyses and transmission electron microscopy (TEM) observations, respectively, established that silicate layers of the clay were intercalated, stacked and randomly distributed in the matrix. Incorporation of very small amounts of oligo(ϵ -caprolactone) (o-PCL) as a compatibilizer in the system leads to a better parallel stacking of the silicate layers¹ and also much stronger flocculation due to the hydroxylated edge–edge interaction of the silicate layers. The intercalated PLA/ C_{18} -mmt nanocomposites exhibited remarkable improvement of mechanical properties in both solid and melt states as compared to that of PLA matrices without clay.

Furthermore, we examined the preparation and characterization of a novel porous ceramic material via burning of PLA/ C_{18} -mmt nanocomposite [20]. This route offers an attractive potential for diversification and application of the polymer–OMLS nanocomposites.

In this paper, first we describe the preparation of PLA-layered silicate nanocomposites by using different type of organically modified mmt. Second, the type of nanocomposites that have been prepared was characterized by using WAXD and TEM. Then we report the improvements of various practical material properties of the nanocomposites such as mechanical properties, HDT, gas permeability, flexural properties, biodegradability in compare to that of neat PLA, and a plausible mechanism of the so fast biodegradation rate of nanocomposites in compare to that of neat PLA. Finally, we report melt rheology of neat PLA and various nanocomposites.

2. Experimental details

2.1. Materials

PLA with D content of 1.1–1.7% was supplied by Unitika Co. Ltd, Japan, and was dried under vacuum at 60 °C and kept under dry nitrogen gas for one week prior to use. The organically modified mmt (C^3C_{18} -mmt) was synthesized by the ion exchange reaction between Na^+ in mmt (CEC = 90 mequiv./100 g), which has original thickness of ~ 1 nm and average length of ~ 100 nm and trimethyl octadecylammonium cation, was supplied by Hojun Yoka Co. Ltd, Japan.

2.2. Nanocomposite preparation

Nanocomposites were prepared by melt extrusion. C^3C_{18} -mmt (powder form) and PLA (pellets form) were first dry-mixed by shaking them in a bag. The mixture was

then melt extruded using twin-screw extruder (PCM-30, Ikegai machinery Co.) operated at 210 °C² (screw speed = 100 rpm, feed rate = 120 g/min) to yield strands of the nanocomposites. Henceforth, the product nanocomposites were abbreviated as PLACNs. PLACNs prepared with three different amount of C^3C_{18} -mmt of 4, 5, and 7 wt% were correspondingly abbreviated as PLACN4, PLACN5 and PLACN7, respectively. The extruded strands were then pelletized and dried under vacuum at 60 °C for 48 h to remove any water. The dried PLACNs pellets were then converted into sheets with a thickness of 0.7–2 mm by pressing with ~ 1.5 MPa at 190 °C for 3 min. The molded sheets were then quickly quenched between glass plates and then annealed at 110 °C for 1.5 h to crystallize isothermally before being subjected to WAXD, TEM, and dynamic mechanical properties measurements.

2.3. Characterization methods

2.3.1. Thermal analysis

The glass transition temperature (T_g), the melting temperature (T_m) and the degree of crystallinity (χ_c) of neat PLA and various PLACNs were determined by a temperature-modulated differential scanning calorimeter (TMDSC) (MDSCTM, TA2920, TA instruments), which was operated at a heating rate of 5 °C/min with a heating/cooling cycle of the modulation period of 60 s and the amplitude of ± 0.769 °C. For the measurement of χ_c , before performing the DSC analysis, we have to subtract the extra heat absorbed by the crystallites formed during heating process from the total endothermic heat flow due to the melting of the whole crystallites. This can be done using TMDSC according to the principles and procedures described in our previous paper [21]. By considering melting enthalpy of 100% crystalline poly(L-lactide) as 93 J/g [22] we have estimated the value of χ_c of neat PLA and various PLACNs, and are presented in Table 1.

2.3.2. Gel permeation chromatography

The weight-average (M_w) and number-average (M_n) molecular weights of the neat PLA and various PLACNs were determined from GPC (LC-VP, Shimadzu Co.), which was based on the calibration using polystyrene standards and tetrahydrofuran (THF)³ as a carrier solvent at 40 °C with flow rate of 0.5 ml/min. The GPC data are also presented in Table 1.

From Table 1, we can see the incorporation of C^3C_{18} -mmt filler into the PLACNs resulted in a reduction of little molecular weight of the matrix. Decreased molecular weight of PLA after nanocomposites preparation may be

² The degradation of intercalated trimethyl octadecylammonium salt was measured by TG analysis. There is no degradation at 210 °C, however, after 272 °C there is 5% weight loss.

³ We first dissolved PLA or PLACNs in chloroform and then diluted with THF.

¹ Upon o-PCL addition the peak position is almost same but intensity increases.

Table 1
Characteristic parameters of neat PLA and various PLACNs

Characteristic parameters	PLA	PLACN4	PLACN5	PLACN7
$M_w \times 10^{-3}$ (g mol ⁻¹)	177	163	169	163
M_w/M_n	1.58	1.61	1.51	1.58
T_m (°C)	168	169.3	169.6	169.7
T_g (°C)	60	59.7	59.6	59.8
χ_c (%)	36	65	56	54
$d_{(001)}$ (nm)	–	3.05	2.85	2.79
D ($\equiv d_{\text{clay}}$) (nm)	–	12.25	12.37	13.27
$D/d_{(001)}$	–	4	4.4	4.8

explained either from the high temperature shear mixing of PLA and C³C₁₈-mmt or due to the presence of ammonium salt in OMLS result some hydrolysis at high temperature.

2.3.3. WAXD

WAXD analyses were performed for the C³C₁₈-mmt powder and three different types of PLACNs using MXlabo diffractometer (MAC Science Co.), which has an X-ray generator of 3 kW, a graphite monochromator, Cu K_α radiation (wavelength, $\lambda = 0.154$ nm) and operated at 40 kV/20 mA. The samples (annealed in case of PLACNs) were scanned in fixed time (FT) mode with counting time of 2 s under the diffraction angle 2θ in the range of 1–70°.

2.3.4. TEM

In order to clarify the nanoscale structure of the various intercalated PLACNs, a TEM (H-7100, Hitachi Co.) was also used and operated at an accelerating voltage of 100 kV. The ultra thin sections (the edge of the sample sheet) with a thickness of 100 nm were microtomed at –80 °C using a Reichert Ultra cut cryoultramicrotome without staining.

2.3.5. Dynamic mechanical analysis

Dynamic mechanical properties of the neat PLA and various PLACNs were measured by using a Reometrics Dynamic Analyzer (RDAII) in the tension–torsion mode. The details were described elsewhere [19].

2.3.6. Flexural properties and HDT

The dried neat PLA and various PLACNs pellets were injection molded to test specimens using an injection machine (IS-80G, Toshiba Machinery Co.) operated at 190 °C with the mold temperature of 30 °C. Flexural modulus and other mechanical properties of the injection-molded specimens (thickness ~ 3.2 mm), annealed at 120 °C for 30 min, were measured according to ASTM D-790 method (Model 2020, Intesco Co.) with strain rate of 2 mm/min at room temperature. We also conducted heat distortion test (Injection molded samples, HDT Tester, Toyoseiki Co.) according to ASTM D-648 method with heating rate of 2 °C/min.

2.3.7. Measurement of gas permeability

Oxygen gas transmission rate of neat PLA and various PLACNs were measured at 20 °C and 90% relative humidity by the ASTM D-1434 differential pressure method (GTR-30XAU, Yanaco Co.). Test samples were prepared by compression molding (thickness ~ 300 μm) and melt quenched amorphous samples were used for this measurement.

2.3.8. Biodegradability study

Biodegradability of the various samples were studied by our own compost instrument at 58 ± 2 °C. The used compost was prepared from bean-curd refuse, food waste compost, and cattle feces, and was supplied by Japan Steel Works, Ltd. The test specimens were prepared by compression molding with a thickness of 1 mm and melt quenched crystallized samples were used for this study. The shape of the original test samples was $3 \times 10 \times 0.1$ cm³.

2.3.9. Melt rheology

Melt rheological measurements were also performed on RDAII instruments with a torque transducer capable of measurements over the range of 0.2–200 g cm. Dynamic oscillatory shear measurements were performed by applying a time dependent strain of $\gamma(t) = \gamma_0 \sin(\omega t)$ and the resultant shear stress is $\sigma(t) = \gamma_0 [G' \sin(\omega t) + G'' \times \cos(\omega t)]$, with G' and G'' being the storage and loss modulus, respectively. Measurements were conducted by using a set of 25 mm diameter parallel plates with a sample thickness of 1–1.5 mm and in the temperature range of 175–205 °C. The strain amplitude was fixed to 5% to obtain reasonable signal intensities even at elevated temperature or low frequency (ω) to avoid the nonlinear response. For each PLACN investigated the limits of linear viscoelasticity were determined by performing strain sweeps at a series of fixed ω s. The master curves were generated by using the principle of time–temperature superposition and shifted to a common reference temperature (T_{ref}) of 175 °C, which was chosen as the most representative of a typical processing temperature of PLA.

3. Results and discussion

3.1. WAXD patterns and TEM observation

The structure of the nanocomposites in the nanometer range has typically been elucidated using WAXD and TEM. WAXD allows a direct evidence of the intercalation of the polymer chains into the silicate galleries. On the other hand, TEM offers a qualitative understanding of the internal structure through direct visualization. Fig. 1 shows the WAXD patterns of C³C₁₈-mmt powder and various representative PLACNs in the range of $2\theta = 1$ –10°. The mean interlayer spacing of the (001) plane (d_{001}) for the C³C₁₈-mmt powder obtained by WAXD measurements is

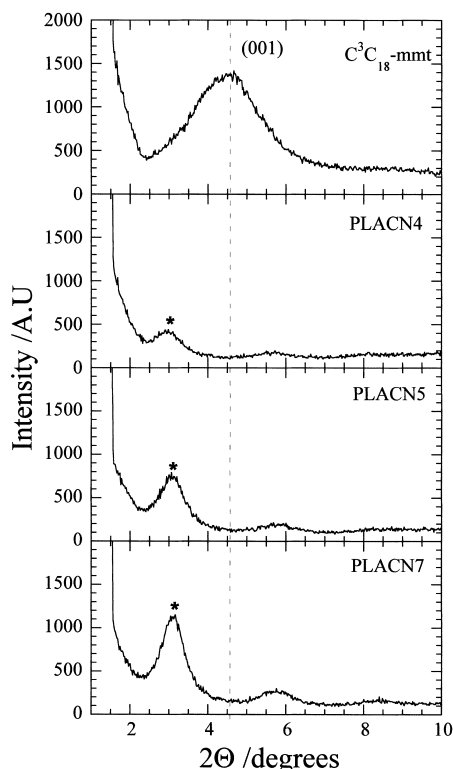


Fig. 1. WAXD patterns for C^3C_{18} -mmt and various PLACNs. The dashed line indicates the location of the silicate (001) reflection of C^3C_{18} -mmt. The asterisks indicate the (001) peak for PLACNs.

1.93 nm ($2\theta \cong 4.56^\circ$). In case of PLACN4, a sharp peak is observed at $2\theta \cong 2.89^\circ$ ($\cong 3.05$ nm), corresponding to the (001) plane of the stacked and intercalated silicate layers dispersed in the PLA-matrix, accompanied with the appearance of very small peak at $2\theta \cong 5.7^\circ$. After calculation, it was confirmed that this peak due to (002) plane (d_{002}) of stacked and intercalated clay homogeneously dispersed in the matrix. With increasing clay content, these peaks become stronger, and shifted towards the higher diffraction angle at $2\theta \cong 3.16$ and 5.75° , respectively, for PLACN7. Note that the existence of sharp Bragg peaks show that the PLACNs still retains an ordered structure after melt mixing although the interlayer spacing increased significantly compared to that of C^3C_{18} -mmt powder. From the WAXD patterns, the crystallite size of intercalated stacked silicate layers of each PLACN is calculated by using Scherrer equation [23,24], i.e. D is given by

$$D = \frac{k\lambda}{\beta \cos \theta} \quad (1)$$

where k is a constant (the value generally = 0.9), λ is the X-ray wave-length (= 0.154 nm), β is the width of the WAXD peak (in radian unit) and is measured by the full width at half maximum, and θ is the WAXD peak position. The calculated value of D for each PLACN is presented in Table 1. It is clearly established that crystallite size, i.e. the thickness ($d_{\text{clay}} \cong D$) of the dispersed stacked silicate layers in the PLACNs gradually increases with clay loading.

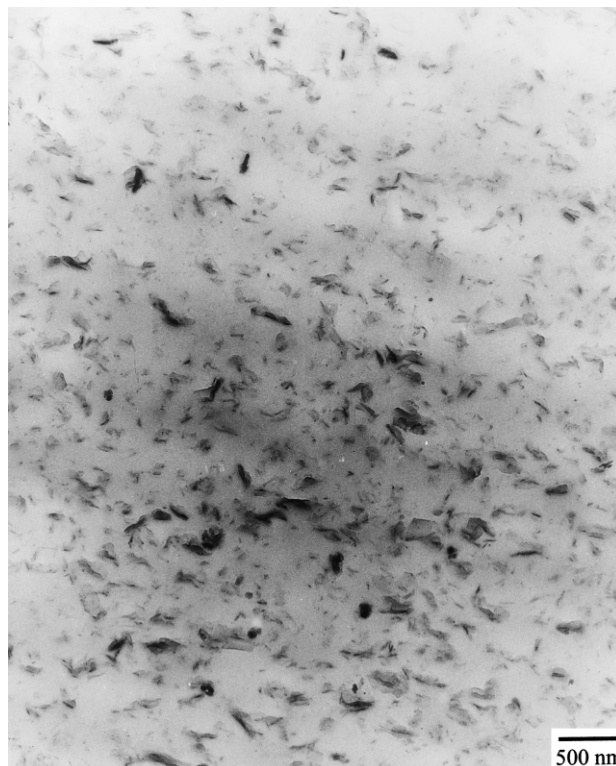


Fig. 2. TEM bright field image of PLACN4. The dark entities are the cross-section of intercalated organoclay layers, and the bright areas are the matrix.

Therefore, we can conclude that the well ordered intercalated PLACNs were formed and coherence order of the silicate layers increases with increasing OMLS. Dividing the value of D by $d_{(001)}$ value of each PLACN, we can estimate the number of the stacked individual silicate layers of about 4 for PLACN4 and PLACN5, and about 5 in case of PLACN7.

The internal structure of the PLACNs in the nanometer scale was observed via TEM analysis. Fig. 2 shows the typical TEM bright field image of PLACN4 in which dark entities are the cross-section of intercalated silicate layers⁴ [25–28]. For PLACN4, we observed large anisotropy of the stacked and flocculated silicate layers, which have an original thickness of ~ 1 nm and average length of ~ 100 nm. The size of some of the flocculated silicate layers appears to reach about 250 nm in length (L_{clay}) owing to the hydroxylated edge–edge interaction of silicate layers, and which are randomly distributed in the PLA matrix. However, we cannot estimate thickness of the stacked silicate layers precisely from the TEM photographs.

In Table 2, we summarized the form factors obtained from TEM images, i.e. average value of L_{clay} thickness ($d_{\text{clay}} \cong D$) of the dispersed clay particles and the correlation length (ξ_{clay}) between them. Combining the

⁴ Since the silicate layers are comprised of heavier elements (Al, Si, O) than the interlayer and surrounding matrix (C, H, N, etc.), they appear darker in bright field image.

Table 2
Comparison of some characteristic parameters between PLACN4 and PLACN2 obtained from TEM, WAXD and DMA measurements

Characteristic parameters	PLACN4	PLACN2 ^a
L_{clay} (nm)	200 ± 25	448 ± 200
ξ_{clay} (nm)	80 ± 20	255 ± 137
L_{clay}/D ($\cong d_{\text{clay}}$)	18	12
$D/d_{(001)}$	4	13
$(G'_{\text{PLACN}}/G'_{\text{PLA}})^b$	1.43	1.65

^a Table 2 in Ref. [19].

^b At 25 °C, G'_{PLA} and G'_{PLACN} are the storage modulus of neat PLA and PLACN, respectively.

results of WAXD analysis and TEM observations, we can estimate another parameter L_{clay}/D , the two-dimensional aspect ratio of the dispersed clay particles. ξ_{clay} value of the PLACN4 is a one order of magnitude lower than the value of L_{clay} , suggesting the formation of ‘spatially linked’ like structure of the dispersed clay particles in the PLA-matrix [19].

Here, we compared the form factors of another intercalated PLACN2 [19] prepared by melt extrusion of PLA and C₁₈-mmt of 4 wt%. For PLACN2, L_{clay} and d_{clay} are in the range of 448 and 38 nm, respectively. The number of the stacked individual silicate layers is about 13 for PLACN2 and ξ_{clay} value of the PLACN2 is in the same order of magnitude compared to that of L_{clay} . Presumably, the poor dispersion of the clay particles for PLACN2 implies the weak interaction of PLA and OMLS due to the poor miscibility between octadecylammonium cation and PLA compared to that of trimethyl octadecylammonium cation and PLA molecules. However, as seen in Table 2, PLACN2 exhibits higher enhancement of the ratio of G' ($G'_{\text{PLACN}}/G'_{\text{PLA}}$), despite the lower aspect ratio L_{clay}/D compared to PLACN4. That is, both the degree of the intercalation of PLA molecules into the space between silicate galleries and the aspect ratio of the dispersed clay particles strongly affected on the final mechanical properties of the PLACNs. The necessity of the intercalating degree of polymer molecules on the enhancement of the mechanical properties was also probed in the intercalated PP–OMLS nanocomposites [21].

3.2. Dynamic mechanical analysis

Dynamic mechanical analysis (DMA) measures the response of a given material to a cyclic deformation (here in tension–torsion mode) as a function of the temperature. DMA results are expressed by three main parameters: (a) the storage modulus (G'), corresponding to the elastic response to the deformation; (b) the loss modulus (G''), corresponding to the plastic response to the deformation, and (c) $\tan \delta$, that is the G''/G' ratio, useful for determining the occurrence of molecular mobility transitions such as the glass transition temperature.

Here DMA analysis has been studied to track the

temperature dependence of storage modulus upon the PLACNs formation. Fig. 3 shows the temperature dependence of G' , G'' and $\tan \delta$ for PLA and corresponding PLACNs. For all the PLACNs, significant enhancement of G' can be seen in the investigated temperature range, indicating intercalated PLACNs have strong influence on the elastic properties of the PLA-matrix.

Below T_g , the enhancement of G' is clear in the intercalated PLACNs. At the temperature range of –20 to 25 °C, the increase in G' are 47% for PLACN4, 52% for PLACN5 and 66% for PLACN7 as compared to that of the neat PLA (Fig. 3). Furthermore, at the temperature range of 80–145 °C all the three nanocomposites exhibit much higher enhancement of G' as compared to that of neat PLA. This is due to the mechanistic reinforcement by clay particles [19,29] at high temperature. Above T_g , when materials become soft reinforcement effect of the clay particles becomes prominent and hence strong enhancement of modulus appeared [10].

On the other hand, above T_g the enhancement of G'' is significant in the intercalated PLACNs in compare to that of below T_g indicating plastic response to the deformation is prominent in the presence of clay when material become soft. However, presence of clay particles does not lead to a significant shift and broadening of the $\tan \delta$ curves for all PLACNs compared to that of neat PLA. This behavior has been ascribed to the unrestricted segmental motions at the organic–inorganic interface neighborhood of intercalated PLACNs.

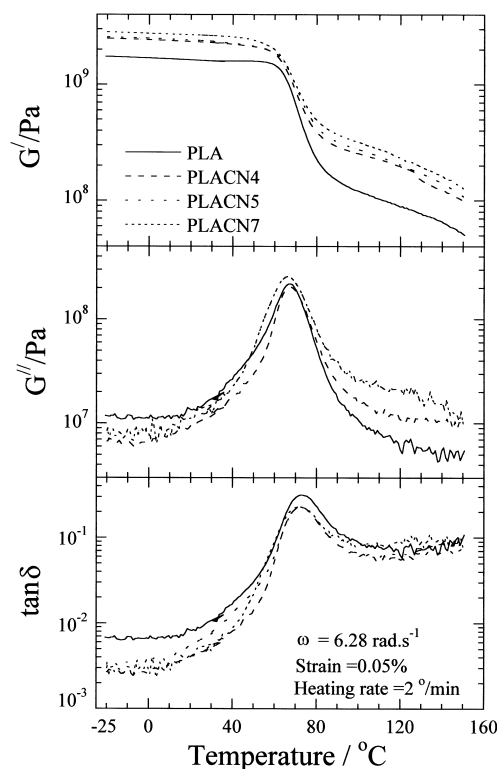


Fig. 3. Temperature dependence of storage modulus (G'), loss modulus (G''), and their ratio ($\tan \delta$) for neat PLA and various PLACNs.

3.3. Flexural properties and HDT

In Table 3, we report the flexural modulus, flexural strength, and distortion at break of neat PLA and various PLACNs measured at 25 °C. There is a significant increase of flexural modulus for PLACN4 compared to that of neat PLA followed by a much slower increase with increasing OMLS content, and a maximum of 21% in case of PLACN7. On the other hand, flexural strength and distortion at break are remarkable increase with PLACN4 then gradually decreases with OMLS loading. This behavior may be due to high OMLS content leads to a brittleness of materials. Therefore, we can control the flexural strength and distortion by increasing or decreasing OMLS content, and incorporation of OMLS of around 4 wt% is the optimum to achieve the high value of flexural strength and distortion.

The nanodispersion of C³C₁₈-mmt in neat PLA also promotes a higher HDT. We examined the HDT of neat PLA and various PLACNs with different load conditions. As seen in Fig. 4(a), in case of PLACN7, there is marked increase of HDT with intermediate load of 0.98 MPa, from 76 °C for the neat PLA to 93 °C for PLACN4. The value of HDT gradually increases with increasing clay content, and in case of PLACN7, the value increases up to 111 °C.

On the other hand, imposed load dependence on HDT is clearly observed in case of PLACNs. Fig. 4(b) shows the typical load dependence in case of PLACN7. The increase of HDT of neat PLA due to nanocomposites preparation is a very important property improvement, not only from the industrial point of view but also molecular control on the silicate layers, that is, crystallization through interaction between PLA molecules and SiO₄ tetrahedral layers.

In case of high load (1.81 MPa), it is very difficult to achieve high HDT enhancement without strong interaction between polymer matrix and OMLS [30]. In case of all PLACNs studied here, the values of T_m (Table 1) do not change significantly as compared to that of neat PLA. Furthermore, in WAXD analyses up to $2\theta = 70^\circ$, we observed no big shifting or formation of new peaks in the crystallized PLACNs. So the improvement of HDT with intermediate load (0.98 MPa) originates from the better mechanical stability of the PLACNs due to mechanical reinforcement by the dispersed clay particles, higher value of χ_c and intercalation. This is qualitatively different from the behavior of Nylon6–OMLS nanocomposites, where the

Table 3
Comparison of materials properties between neat PLA and various PLACNs

Materials properties	PLA	PLACN4	PLACN5	PLACN7
Modulus (GPa)	4.8	5.5	5.6	5.8
Strength (MPa)	86	134	122	105
Distortion at break (%)	1.9	3.1	2.6	2
$P_{\text{PLACN}}/P_{\text{PLA}}$	1	0.88	0.85	0.81

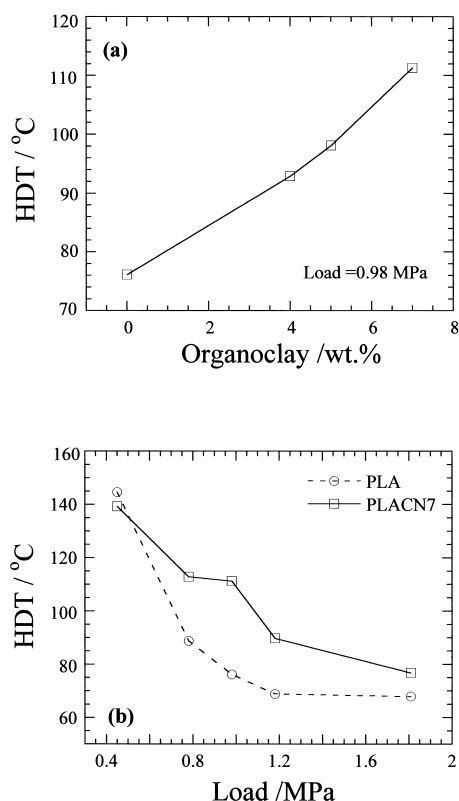


Fig. 4. (a) Organoclay (wt%) dependence of HDT of neat PLA and various PLACNs. (b) Load dependence of HDT of neat PLA and PLACN7.

mmt layers stabilize in a different crystalline phase than that found in the neat Nylon6, with a higher HDT [31].

3.4. Oxygen gas permeability

The nanoclays are believed to increase the gas barrier properties by creating a maze or ‘tortuous path’ that retard the progress of gas molecules through the matrix resin [9,32, 33,34]. The O₂ gas permeability’s for the neat PLA and various PLACNs are presented in Table 3. According to the Nielsen model [35], platelets of length ($\cong L_{\text{clay}}$) and width ($\cong D_{\text{clay}}$) of the clay, which are dispersed parallel in polymer matrix, then the tortuosity factor (τ) can be expressed as

$$\tau = 1 + (L_{\text{clay}}/2D_{\text{clay}})\phi_{\text{clay}} \quad (2)$$

where ϕ_{clay} is the volume fraction of dispersed clay particles. Therefore, the relative permeability coefficient ($P_{\text{PLACN}}/P_{\text{PLA}}$) is given by

$$\frac{P_{\text{PLACN}}}{P_{\text{PLA}}} = \tau^{-1} = \frac{1}{1 + (L_{\text{clay}}/2D_{\text{clay}})\phi_{\text{clay}}} \quad (3)$$

where P_{PLACN} and P_{PLA} are the permeability coefficient of PLACN and neat PLA, respectively. We consider here PLACN4, with value of $L_{\text{clay}} = 200$ nm (from TEM), and the value of $D_{\text{clay}} = 12.25$ nm as calculated by using Scherrer equation [23,24]. Therefore, the calculated value of $P_{\text{PLACN}}/P_{\text{PLA}}$ for PLACN4 is equal to 0.896. The

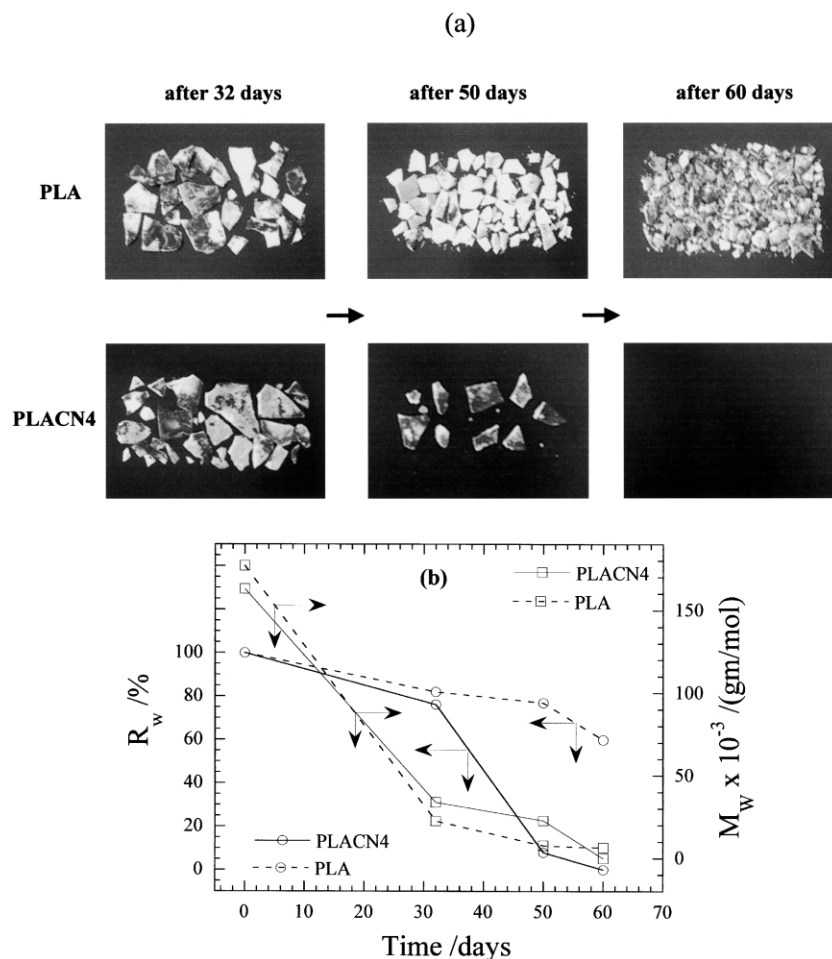


Fig. 5. (a) Real pictures of biodegradability of neat PLA and PLACN4 recovered from compost with time. Initial shape of the crystallized samples was $3 \times 10 \times 0.1 \text{ cm}^3$. (b) Time dependence of residual weight, R_w and of matrix, M_w of PLA and PLACN4 under compost.

experimental value of 0.885 is well matched with the above model but slightly lower than the calculated one. Presumably, the planer orientation of the dispersed clay particles in the compress-molding sheet is not sufficient.

3.5. Biodegradability

The most interesting and exciting aspect of this research is the significant improvement of biodegradability of neat PLA after nanocomposites preparation. Very recently, Lee et al. [36] reported the biodegradation of aliphatic polyester based nanocomposites under compost. They assumed that the retardation of biodegradation due to the improvement of the barrier properties of the aliphatic polyester after nanocomposites preparation with clay. However, there is no data about permeability.

Fig. 5(a) shows the real pictures of the recovered samples of neat PLA and PLACN4 from compost with time. The decreased M_w and residual weight R_w percentage of the initial test samples with time is also shown in Fig. 5(b). Obviously, the biodegradability of neat PLA is significantly enhanced after nanocomposites preparation with C^3C_{18} -mnt. Within one month, both the extent of M_w and the

extent of weight loss are almost same level for both neat PLA and PLACN4.⁵ However, after one month, a sharp change occurs in weight loss of PLACN4, and within two months, it is completely degraded by compost. The degradation of PLA under compost is a complex process involving four main phenomena, namely: water absorption, ester cleavage and formation of oligomer fragments, solubilization of oligomer fragments, and finally diffusion of soluble oligomers by bacteria [37]. Therefore, the factor, which increases the hydrolysis tendency of neat PLA, ultimately controls the degradation of PLA. However, from Fig. 5(b) it is found that the hydrolysis tendency of PLA and PLACN4 is almost same.

⁵ Actually, M_w of PLACN4, which was initially lower than that of neat PLA even become little higher than that of neat PLA after 32–50 days compost while weight loss of PLACN4 is very sharp compared to that of neat PLA. In case of PLACN4 there are some intercalated PLA and also surroundings PLA, and we believe these intercalated PLA chains are more stable and retain its high M_w towards compost. Since intercalated PLA has high M_w than that of surrounding, and average M_w appeared to be little high compared to that of matrix. For this reason the M_w of PLACN4 appeared to be high although weight change is very sharp within 50 days compared to that of neat PLA.

We expect that the presence of terminal hydroxylated edge groups of the silicate layers may be one of the responsible factors for this behavior. In case of PLACN4, the stacked (~ 4 layers) and intercalated silicate layers are homogeneously dispersed in the PLA matrix (from TEM image) and these hydroxy groups start heterogeneous hydrolysis of the PLA matrix after absorbing water from compost. This process takes some time to start. For this reason, the weight loss and degree of hydrolysis of PLA and PLACN4 is almost same up to one month (Fig. 5(b)). However, after one month there is a sharp weight loss in case of PLACN4 compared to that of PLA. That means one month is a critical value to start heterogeneous hydrolysis, and due to this type of hydrolysis matrix becomes very small fragments and disappear with compost. This assumption was confirmed by conducting same type of experiment with PLACN prepared by using dimethyl dioctdecylammonium salt modified synthetic mica which has no terminal hydroxylated edge group, and the degradation tendency almost same with PLA.

3.6. Melt rheology

The measurement of rheological properties of polymeric materials under molten state is crucial to gain a fundamental understanding of the nature of the processability and the structure–property relationship for these materials. The linear dynamic viscoelastic master curves for the neat PLA and various PLACNs are shown in Fig. 6. The master curves were generated by applying time–temperature superposition principle and shifted to a common temperature of 175 °C using both frequency shift factor (a_T) and modulus shift factor (b_T).

As expected, the moduli of the nanocomposites increases with increasing clay loading at all frequencies. At high frequencies, the qualitative behavior of $G'(\omega)$ and $G''(\omega)$ is essentially same and unaffected with frequencies. However, at low frequencies $G'(\omega)$ and $G''(\omega)$ increase monotonically with increasing clay content. In the low frequency region, the curves can be expressed by power-law of $G'(\omega) \propto \omega^2$ and $G''(\omega) \propto \omega$ for PLA, suggesting that this is similar to those of the narrow M_w distribution homopolymer melts. On the other hand, for $a_T\omega < 5 \text{ rad s}^{-1}$, viscoelastic response [particularly $G'(\omega)$] for all the nanocomposites displays significantly diminished frequency dependence as compared to the matrix. In fact, for all PLACNs, $G'(\omega)$ becomes nearly independent at low $a_T\omega$ and exceeds $G''(\omega)$, characteristic of materials exhibiting a pseudo-solid like behavior [38]. The terminal zone slope values of both neat PLA and PLACNs are estimated at lower $a_T\omega$ region ($< 10 \text{ rad s}^{-1}$), and are presented in Table 4. The lower slope values and the higher absolute values of the dynamic moduli indicate the formation of ‘spatially linked’ structure (also observed from TEM photograph) in the PLACNs under molten [19,39]. Because of this structure or highly geometric constraints, the individual stacked silicate layers

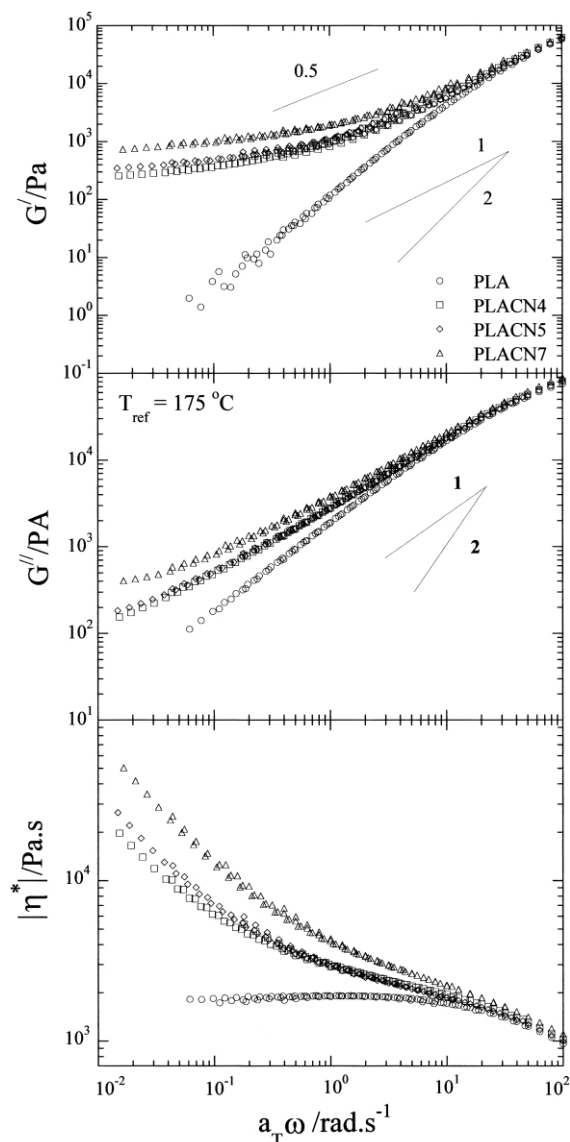


Fig. 6. Reduced frequency dependence of storage modulus [$G'(\omega)$], loss modulus [$G''(\omega)$], and complex viscosity [$|\eta^*(\omega)|$] of neat PLA and various PLACNs.

are incapable of freely rotating and hence by imposing small $a_T\omega$, the relaxations of the structure are prevented almost completely. This type of prevented relaxation due to the highly geometric constraints of the stacked and intercalated silicate layers lead to the presence of the pseudo-solid like behavior as observed in PLACNs [40].

Table 4
Terminal slopes of G' and G'' vs $a_T\omega$ ($< 10 \text{ rad s}^{-1}$) for neat PLA and various PLACNs

Sample	G'	G''
PLA	1.6	0.9
PLACN4	0.2	0.5
PLACN5	0.18	0.4
PLACN7	0.17	0.32

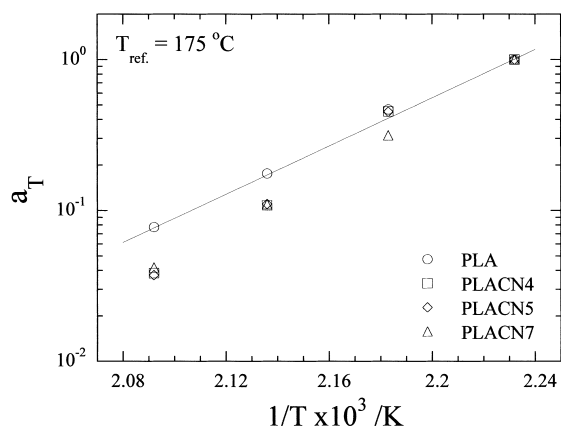


Fig. 7. Frequency shift factors (a_T) as a function of temperature.

The dynamic complex viscosity [$|\eta^*(\omega)|$] master curves for the neat PLA and various PLACNs, based on linear dynamic oscillatory shear measurements are also shown in Fig. 6. From Fig. 6, we can see at low $a_T\omega$ region ($<10 \text{ rad s}^{-1}$) the neat PLA exhibits almost Newtonian behavior while all PLACNs show very strong shear-thinning tendency. We believe this behavior comes from nature of the clay particles, which are dispersed in the PLA matrix.

In our previous study on lyophilized smectic clay–toluene suspensions [41], we observed this type of shear-thinning feature of the clay particles in the rapid shear flow. Such a feature is strongly dependent on the shear rate in the dynamic measurements because of the formation of the shear-induced alignment of the dispersed clay particles.

The temperature dependence frequency shift factor (a_T , WLF type [42]) used to generate master curves shown in Fig. 6 are shown in Fig. 7. The dependence of the frequency shift factors on the silicate loading suggests that the temperature-dependent relaxations process observed in the viscoelastic measurements are somehow affected by the presence of the silicate layers [38].

4. Conclusions

We have successfully prepared new and novel biodegradable PLA-layered silicate nanocomposites by simple melt extrusion of PLA and $\text{C}^3\text{C}_{18}\text{-mmt}$, wherein silicate layers of the clay were intercalated, stacked (~ 4 to 5 layers), and nicely distributed in the PLA-matrix. These systems were the first successful biodegradable intercalated PLA-layered silicate nanocomposites. All the nanocomposites exhibited remarkable improvements of material properties such as mechanical properties both in solid and melt state, flexural properties, HDT, gas permeability compared to that of pristine, with simultaneous improvement in biodegradability of PLA. These concurrent property improvements are well beyond what can be generally achieved through the micro/macro-composites preparation or chemical modification of neat PLA.

Acknowledgements

SSR thanks Japan Society for the Promotion of Science (JSPS) for financial support in terms of Post Doctoral Fellowship (ID NO. P02152). We express our appreciation to the reviewer for his constructive and meticulous assessment of the manuscript.

References

- [1] Grijpma DW, Pennings AJ. *Macromol Chem Phys* 1994;195:1649.
- [2] Perego G, Cella GD, Bastioli C. *J Appl Polym Sci* 1996;59:37.
- [3] Sinclair RG. *J Macromol Sci, Pure Appl Chem* 1996;A33:585.
- [4] Tsuji H, Ikada Y. *J Appl Polym Sci* 1998;67:405.
- [5] Martin O, Averous L. *Polymer* 2001;42:6209.
- [6] Lunt J. *Polym Degrad Stab* 1998;59:145.
- [7] Fang Qi, Hanna MA. *Ind Crops Pds* 1999;10:47.
- [8] Ogata N, Jimenez G, Kawai H, Ogihara T. *J Polym Sci, Polym Phys* 1997;35:389.
- [9] Messersmith PB, Giannelis EP. *Chem Mater* 1994;6:1719.
- [10] Usuki A, Kawasumi M, Kojima Y, Okada A, Kurauchi T, Kamigaito O. *J Mater Res* 1993;8:1174.
- [11] LeBaron PC, Wang Z, Pinnavaia TJ. *Appl Clay Sci* 1999;15:11.
- [12] Giannelis EP, Krishnamoorti R, Manias E. *Adv Polym Sci* 1999;138:107.
- [13] Alexander M, Dubois P. *Mater Sci Engng* 2000;28:1.
- [14] Biswas M, Sinha Ray S. *Adv Polym Sci* 2001;155:167.
- [15] Okamoto M, Nam PH, Maiti P, Kotaka T, Hasegawa N, Usuki A. *Nano Lett* 2001;1:295.
- [16] Okamoto M, Nam PH, Maiti P, Kotaka T, Nakayama T, Takada M, Ohshima M, Usuki A, Hasegawa N, Okamoto H. *Nano Lett* 2001;1:503.
- [17] Vaia RA, Giannelis EP. *Macromolecules* 1997;30:8000.
- [18] Krishnamoorti R, Vaia R, Giannelis EP. *Chem Mater* 1996;8:1728.
- [19] Sinha Ray S, Maiti P, Okamoto M, Yamada K, Ueda K. *Macromolecules* 2002;35:3104.
- [20] Sinha Ray S, Okamoto K, Yamada K, Okamoto M. *Nano Lett* 2002;2:423.
- [21] Nam PH, Maiti P, Okamoto M, Kotaka T, Hasegawa N, Usuki A. *Polymer* 2001;42:9633.
- [22] Fischer EW, Sterzel HJ, Wegner G. *Kolloid-Z Z Polym* 1973;25:980.
- [23] Dritis VA, Tchoubar C. *X-ray diffraction by disordered lamellar structures*, vol. 99. New York: Springer; 1990. p. 21–2.
- [24] Cullity BD. *Principles of X-ray diffraction*. Reading, MA: Addison-Wesley; 1978.
- [25] Klimentidis RE, Mackinnon IDR. *Clays Clay Miner* 1986;34:155.
- [26] Grim RE. *Clay mineralogy*. New York: McGraw-Hill; 1953.
- [27] Pinnavaia TJ. In: Legrand AP, Flandrois S, editors. *Chemical physics of intercalation*. New York: Plenum Press; 1987.
- [28] Güven N. In: Bailey SW, editor. *Hydrous phyllosilicates*. Reviews in mineralogy, Washington, DC: Mineralogical Society of America; 1988.
- [29] Sinha Ray S, Okamoto K, Maiti P, Okamoto M. *J Nanosci Nanotechnol* 2002;2:471.
- [30] Kojima Y, Usuki A, Kawasumi M, Okada A, Fukushima Y, Kurauchi T, Kamigaito O. *J Mater Res* 1993;8:1179.
- [31] Kojima Y, Usuki A, Kawasumi M, Okada A, Kurauchi T, Kamigaito O. *J Polym Sci, Polym Chem* 1993;31:983.
- [32] Yano K, Usuki A, Okada A, Kurauchi T, Kamigaito O. *J Polym Sci, Polym Chem* 1993;31:2493.
- [33] Usuki A, Kawasumi M, Kojima Y, Okada A, Kurauchi T, Kamigaito O. *J Mater Res* 1993;8:1185.
- [34] Xu R, Manias E, Snyder AJ, Runt J. *Macromolecules* 2001;34:337.

- [35] Nielsen L. *J Macromol Sci Chem* 1967;A1(5):929.
- [36] Lee SR, Park HM, Lim H, Kang T, Li X, Cho WJ, Ha CS. *Polymer* 2002;43:2495.
- [37] Liu JW, Zhao Q, Wan CX. *Space Med Med Engng* 2001;14:308.
- [38] Krishnamoorti R, Giannelis EP. *Macromolecules* 1997;30:4097.
- [39] Ren J, Silva AS, Krishnamoorti R. *Macromolecules* 2000;33:3739.
- [40] Hoffmann B, Kressler J, Stoppelmann G, Friedrich Chr, Kim GM. *Colloid Polym Sci* 2000;278:629.
- [41] Okamoto M, Taguchi H, Sato H, Kotaka T, Tatayama H. *Langmuir* 2000;16:4055.
- [42] Williams ML, Landel RF, Ferry JD. *J Am Chem Soc* 1955;77:3701.